Journal of Molecular Modeling (2020) 26: 116
https://doi.org/10.1007/s00894-020-04389-2

ORIGINAL PAPER

A DFT study of isolated histidine interactions with metal ions (Ni^{2+}, Cu^{2+}, Zn^{2+}) in a six-coordinated octahedral complex

Latasha M. Franklin[1] · Sharnek M. Walker[1] · Glake Hill[1]

Received: 9 March 2020 / Accepted: 22 April 2020 / Published online: 6 May 2020

Abstract

Understanding the role that metal ions play in biological and material processes is critical to addressing a number of diseases and problems facing society today. There have been a number of studies that have begun to approach this concern from a myriad of different perspectives. However, there is still a considerable lack of understanding concerning the mechanisms and structures of metal-related problems, specifically biological and medical-related issues. Understanding the mechanism of ingestion and uptake of metals into the human body is critical to addressing many diseases such as Alzheimer's and certain types of cancers. Using computational techniques, this work adds to the overall understanding of metal interactions with proteins by focusing on metal ion interactions with the amino acid, histidine, one of the most common sites of metal attachment. In this work, the geometries of single and dual histidines attached to Ni^{2+}, Cu^{2+}, and Zn^{2+} ions at B3LYP/6-311G(d) are presented. The results show stable octahedral complexes associated with each of the metal ions. Free energy calculations suggest that all three complexes are spontaneous in the formation of the dual histidine-metal complexes. Nickel and copper are spontaneous in the formation of the single histidine complex, although the copper complex undergoes slight geometric changes. Zinc is found to be nonspontaneous in forming the single histidine complex. Finally, the reduction potential of the single histidine-metal complex is presented. All of the complexes show positive reduction potentials. However, the nickel and copper complexes undergo geometrical changes to adopt a square planar conformation.

Keywords Density functional theory · Histidine · Metal ions · Reduction potentials · Free energy of reaction

Introduction

The role of metals in today's society has become increasingly important [1]. A number of applications focusing on utilizing metals, specifically metal cations, as their central component, have filled a spectrum from mechanical and technological uses [2–5] to medical and pharmaceutical treatments [6–8]. Metals have critical catalytic properties that make their inclusion in new materials and processes vital [9]. In addition, metal cations have been the foundation on which antifungal and antibacterial compounds have been built [10]. Therefore, undoubtedly, metals are critical to future innovations and discoveries.

However, the ubiquitous role of metals in society and their increasing amounts have also caused potential problems for the environment [11]. Thus, landfills and waste sites are becoming filled with metal-containing compounds and materials, which leads to increased leaching into the soil and water table. This, in turn, increases the amount of metal cations found within plants, drinking water, and animals, which depend on both of these.

This can potentially affect humans because of the reliance of humans on both water and animals/plants for survival. These metal cations, through both the environment and current pharmaceutical approaches, can be introduced into the body and subsequently the bloodstream. This introduction of metal cations into the bloodstream can potentially lead to neurological disease, cell damage, and oncogenesis, as well as other less-understood effects.

Upon entry into the human bloodstream, one of the most likely sites of interactions is with blood-born proteins [1, 12]. Amino acids provide good opportunities for protein-metal complexes due to the reactive nature of the R group side

✉ Glake Hill
glakeh@icnanotox.org

[1] Department of Chemistry, Physics, and Atmospheric Sciences, Jackson State University, Jackson, MS 39217, USA

chains, as well as free amine and carboxyl groups. Binding of metal cations onto the proteins found within the body can cause normal cellular process to be inhibited [13, 14], the creation of free radicals through increased redox reactions [15–17], or disruption of structural components through geometrical changes.

For example, metal ions have been strongly suggested to be a component in the development of Alzheimer's disease [18–21]. An aggregate of the amyloid β-peptide is thought to be responsible for the disease [22–24]. This aggregation may potentially be caused by metal ions coagulating these neurological proteins. Studies have shown that high levels of metal ions are present in the tissues of those that have this disease [25]. Aggregation and potential oxidation reaction [26] can possibly be the direct cause of diminished neurological functions and the progression of this Alzheimer's disease [27]. These types of interactions between proteins and metal ions may also play a part in other neurological diseases and complications throughout the body [28].

Therefore, it is critical to gain greater understanding of the mechanisms of how metal cations interact with cellular components to affect biological functions. Current approaches have provided some insight into metal cation behavior in vivo. Studies have focused on histidine and cysteine as primary sites of metal complex binding. Cysteine, although not the subject of this work, is an attractive site for metal ion binding due to the sulfur located on its R side chain. Histidine, the subject of this work, contains an imidazole side group that can also participate in the binding metal ions. Consequently, a number of metalloproteins contain histidine as the primary site of metal ion coordination.

A number of studies have focused on understanding the basic structure of the interactions of histidine with these metal ions. Kong et al. focused on understanding the role that metal ions play in complexing the previously mentioned amyloid proteins by providing IR spectra and structural information about these metal complexes and their interactions with histidine dimers, specifically His13 and His14 [29]. Pushie et al. have focused on metal ions interacting with imidazole to mimic the side chain of histidine [30]. Han et al. concurred that the imidazole was a major component of the metal-histidine interaction [31]. Potocki et al. studied the metal ions within the TjZNT1 ZIP transporters and also determined the site of metal binding to be predominately on the imidazole [32]. However, the structures were limited in their interactions with the ion because the histidine was often in complex proteins with the amino terminal and the carboxyl terminal occupied with peptide bonding. Even with this limitation, there is disagreement as to the structural geometries of the metal ions, specifically, whether the complex adopts octahedral-type geometries, or a square planar-type structure. This distinction could explain structural changes in the proteins to which the metal is attached.

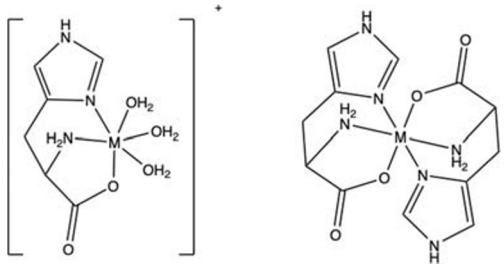

Fig. 1 Proposed structure of the histidine-metal complex with single histidine and dual histidine (M=Ni^{2+}, Cu^{2+}, or Zn^{2+})

Others have taken an isolated histidine approach to determine the appropriate structures. These studies have focus on complexing single histidines with metal cations to predict the geometry of the complex. Yet, even with the isolated histidines, there is disagreement as to the structure of the histidine with the complexes. In isolation, Umadevi et al. suggested that the structure of the metal with the two histidines attaches to the metal ions via two ligands each, creating a square planar-like conformation [33]. This is complemented with a water molecule attached to the metal.

Other work suggests that there is another possible structure to be considered. Gorboletova et al. have suggested a complex where each of the histidines attaches via three ligands (NH_2, COO^-, and the imidazole) [34]. This octahedral structure is supported by complexes of metal ions with other compounds, such as ethylenediaminetetraacetic acid (EDTA) [35] or diethylenetriaminepentaacetic acid (DTPA) [36]. In this work, it is suggested that this structure may be critical in the understanding of the mechanism of metal ion interaction in biological species. The six-ligand octahedral complex of metal ions (Ni^{2+}, Cu^{2+}, and Zn^{2+}) with single and dual histidine (Fig. 1) is explored using *ab initio* methods, and insights into the thermodynamics of the reactions of these complexes are discussed.

Computational details

All geometries were optimized using Gaussian16 [37] and the DFT functional B3LYP [38, 39] with a 6-311G(d) basis set. All structures were optimized without any geometrical constraints. Local minima of all

Table 1 The relative energy of spin states (kcal/mol) for the $M(H_2O)_6$

	The two lowest spin states	Lower spin state	Higher spin state
Ni^{2+}	Singlet, triplet	47.83	0
Cu^{2+}	Doublet, quartet	0	156.56
Zn^{2+}	Singlet, triplet	0	165.97

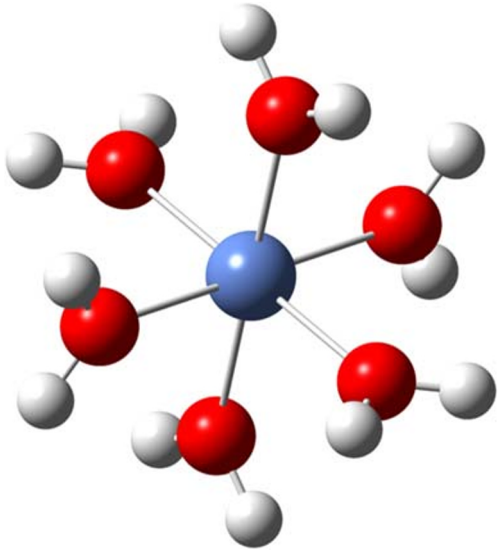

Fig. 2 $M(H_2O)_6^{2+}$, where M=Ni^{2+}, Cu^{2+}, or Zn^{2+}

structures were verified using frequency calculations. Gaussview6 [40] was used to visualize all structures. The lowest two spin states for each of the metal complexes were calculated, and the relative energies are presented in Table 1. As indicated, Ni^{2+} preferred the higher triplet state in each of the complexes, while Cu^{2+} and Zn^{2+} preferred the lower spin state, doublet, and singlet, respectively.

Using these gas phase calculations and the appropriate spin state, the free energy of solvation was calculated using the solvation model based on density (SMD) [41]. The gas phase free energy was calculated as:

$$\Delta G_{\mathrm{hyd}} = \Delta G_{\mathrm{gas}} + \Delta\Delta G_{\mathrm{sol}}$$

where ΔG_{hyd} is the free energy of the reaction in aqueous environment, ΔG_{gas} is the free energy calculation via gas phase methods, and $\Delta\Delta G_{\mathrm{sol}}$ is the difference between the free energy of solvation of the reactants and the products using SMD. The thermodynamic cycle used for each stage will be presented in the "Results and discussion" section.

Table 2 Free energy of hydration for metal cations at B3LYP/6-311G(d), using the SMD

	Ni^{2+}	Cu^{2+}	Zn^{2+}
ΔG(gas)	− 317.69	− 318.19	− 305.45
ΔG(solv)	− 179.25	− 187.24	− 187.08
ΔG(aq)	− 496.94	− 505.44	− 492.53
Other theor.[a]	− 480.81	− 480.06	− 458.58
Exp.[a]	− 477.50	− 481.80	− 469.20

[a] Chen et al. [35]

Results and discussion

Hydration of metal ions

Following the methodology suggested in similar studies [35], metal ion reactions with water were calculated to determine the free energy of solvation. This approach better models the biological environment that a metal ion would experience in a water solvent. The solvation of the metal ion is described both explicitly and implicitly. The first solvation shell is described by placing water molecules around the ion in an octahedral configuration (Fig. 2). The remaining solvation is implicitly described using the SMD. This approach is in alignment with previous work done with metal ion solvation.

To determine the free energy for the reaction, an optimized cluster of six water molecules was used instead of the energy of one water molecule multiplied by six. This allows for better correlation with experimental results for the free energy of hydration for the ions. It also provides better comparison with the work presented by Chen [35]. The thermodynamic cycle to determine the free energy is given in Fig. 3:

Once again, the free energy of hydration (ΔG_{hyd}) is determined by the equation:

$$\Delta G_{\mathrm{hyd}} = \Delta G_{\mathrm{gas}} + \Delta\Delta G_{\mathrm{sol}}$$

where ΔG(gas) is determined by

$$\Delta G_{\mathrm{gas}} = G_{\mathrm{gas}}\left[\mathrm{M(H_2O)_6}^{2+}\right] - G_{\mathrm{gas}}\left[(\mathrm{H_2O})_6\right]$$

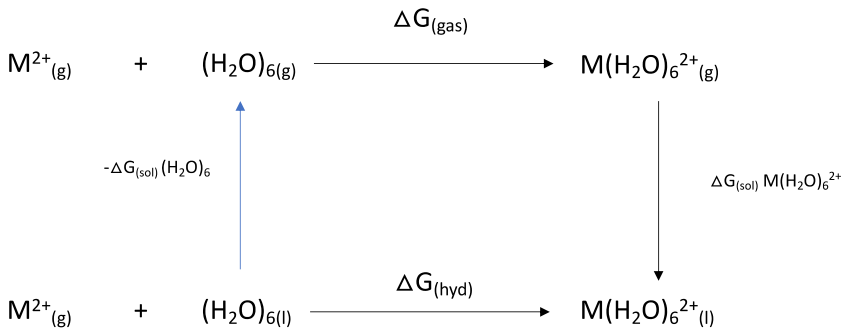

Fig. 3 The thermodynamic cycle for the hydration of the metal ion

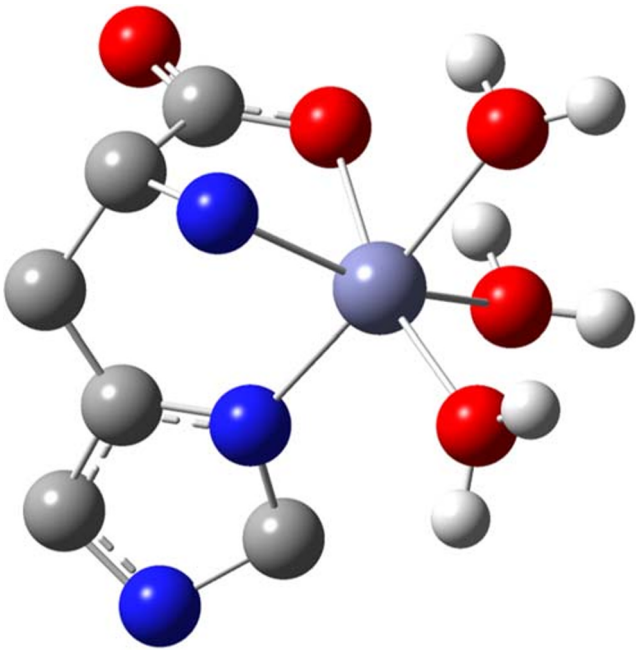

Fig. 4 The optimized structure of the single histidine-metal complex (where M=Ni2+, Zn2+) and water molecules (hydrogen was removed from histidine for clarity)

The $\Delta\Delta G$ is determined by

$$\Delta\Delta G_{sol} = \Delta G_{sol}\left[M(H_2O)_6{}^{2+}\right] - \Delta G_{sol}\left[(H_2O)_6\right]$$

The results of these calculations are found in Table 2. The results are also compared with other theoretical results and available experimental results. The calculated results are in relatively good agreement with the experimental results. Although this work presents calculated results that are between 4 and 5% below the experimental results, they are in good agreement with the other previous theoretical results by Chen et al. [35]. There are small differences between Chen and these results due to the difference in the basis set (LanL2DZ for Chen, 6-311G(d) this work) as well as the inclusion of BSSE in the work of Chen, but not included in this present work. Those distinctions account for the small differences in the theoretical results.

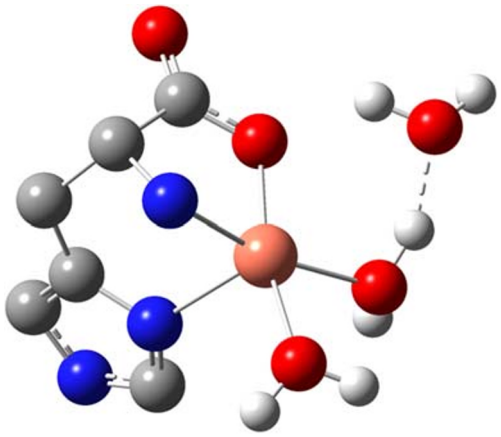

Fig. 5 The optimized structure of the single histidine-Cu complex and water molecules (hydrogen was removed from histidine for clarity)

The utilization of the 6-311G(d) basis set does yield the correct relative order of the metal ions, while the LanL2DZ basis set gives roughly equal free energy of hydration for Ni^{2+} and Cu^{2+}. Both experimental results and the results of this work suggest that Ni^{2+} has a higher free energy of hydration than Cu^{2+}. LanL2DZ performed by others gives equal free energies.

Formation and energetics of $M(His)(H_2O)_3{}^+$

The reaction of the hydrated metal ions with a single histidine was subsequently modeled. The histidine is complexed with the metal ion using three ligands (Fig. 4) with the water

Table 3 Geometric parameters for $M(His)(H_2O)^+$ complexes and $M(His)_2$ complexes (in angstroms, angles and dihedrals are in degrees)

Metals	M-H_2O[a]	COO-M	NH_3-M	HisN-M	COO-M-NH_3	NH_3-M-HisN	COO-M-HisN	HisN-COO-M-NH_3
$M(His)(H2O)_3{}^+$ Complexes								
Ni^{2+}	2.12	1.98	2.07	2.05	81.9	90.4	94.6	94.6
Cu^{2+}	2.01, 3.57[b]	1.92	2.01	2.26	82.4	90.1	95.2	95.2
Zn^{2+}	2.16	2.03	2.14	2.08	79.6	88.3	99.4	99.9
$M(His)_2$								
Ni^{2+}	-	2.02	2.12	2.16	80.9	82.2	92.4	93.7
Cu^{2+}	-	1.92	2.02	2.69	84.4	76.3	87.5	88.8
Zn^{2+}	-	2.01	2.18	2.28	80.0	80.1	91.8	93.6

[a] This is the average distance for all of the water-metal distances

[b] This is an outlier distance of the water molecule

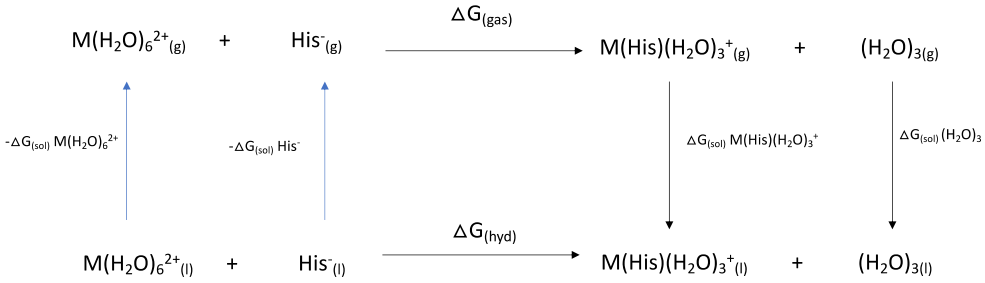

Fig. 6 The thermodynamic cycle for the reaction $M(H_2O)_6^{2+} + His^- \rightarrow M(His)(3H_2O)^- + 3H_2O$

molecules in place to maintain the octahedral geometry. The geometric parameters are listed in Table 3. The bond distances, angles, and dihedral angles of the nickel and zinc complexes are similar to one another, differing by only a few angstroms or degrees. The structure maintains an octahedral-type ligand bonding between the amine, carboxyl, and imidazole sites on the histidine while maintaining the attraction of the water molecules.

Copper's geometry is significantly different from the other two metal ion complexes (Fig. 5). The most noticeable difference is in the imidazole metal ion attraction. The distance between the two increases compared with that of the other two metals. The imidazole moves farther from the metal while the other two ligands (NH_2 and COO^-) become more closely attached to the metal. Also, one of the water molecules that is attached to the metal to complete the octahedral geometry in the other metals moves from this position within the optimized copper complex. This water molecule moves outside of the first solvation shell into perhaps a secondary shell. It must be noted that the copper is in the doublet state throughout this optimization. When optimized in the quartet state, even though it is not the lower energy, it maintains the octahedral geometry of the other ions. This geometric difference is not unexpected. This seems to be in line with the Jahn-Teller effect that is expected to be present in other copper complexes.

To address how these single histidine-metal complexes are formed, the free energy of reaction was determined for the reaction of the hydrated metal ion and the histidine. These free energies were once again calculated in the same manner as before but with the thermodynamic cycle given in Fig. 6.

When comparing the free energy of reactions for the metals (Table 4), a general trend appears. As the atomic number increases, the free energy of reaction becomes more positive. The nickel and the copper ions are shown to be spontaneous reactions predicted to be thermodynamically favored. The zinc ion, however, is predicted to be nonspontaneous and thermodynamically unfavored. This is not due to the inclusion of the hydration model since the free energy of solvation is consistent with the other metal ions. The gas phase free energy, while still negative, is considerably less negative than the other metal ions. This combination of more positive gas phase free energy along with the lowest free energy of solvation gives rise to a positive free energy of reaction.

Table 4 Free energy of reaction for the reaction: $M(H_2O)_6^{2+} + His^- \rightarrow M(His)(3H_2O)^- + 3H_2O$, B3LYP/6-311G(d), with SMD

Metal	ΔG(gas)	ΔG(solv)	ΔG(aq)
Ni^{2+}	− 207.43	185.32	− 22.11
Cu^{2+}	− 217.81	191.29	− 26.52
Zn^{2+}	− 124.74	192.58	67.84

Formation and energetics of $M(His)_2$

The octahedral structure of the metal complex with two histidines (Fig. 7) was studied and compared with the metal ion with the one histidine. These are also presented in Table 3. The geometries for all three of the dual histidine-metal complexes were slightly different than the geometries of the single histidine-metal complexes. The addition of the second histidine caused the structures to adopt a slightly strained octahedral geometry. The ligands of the histidines have longer bond distances and smaller angles, suggesting an elongation of the histidines away from the metal and greater strain in the bend of the histidines.

Once again, copper shows an exaggerated geometry that is potentially due to Jahn-Teller effects. The copper histidine complex had smaller metal ligand bonds than the other metals but the angles between the ligands were smaller suggesting a

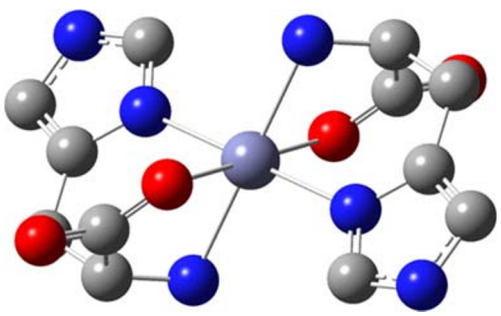

Fig. 7 The optimized structure of the dual histidine-metal complex and water molecules (hydrogen was removed from histidine for clarity)

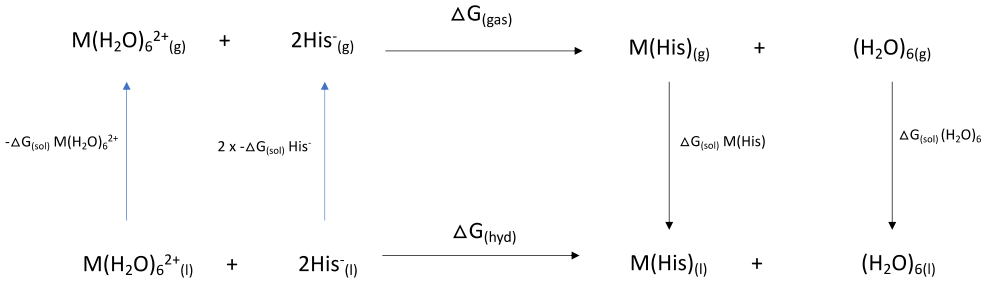

Fig. 8 The thermodynamic cycle for the reaction $M(H_2O)_6^{2+} + 2His^- \rightarrow M(His)_2 + 6H_2O$

greater shift away from the octahedral geometry. Also, as was the case with the single histidine complex, the imidazole rings of the histidines were extended away from the copper center. In comparison with the other metals, the imidazole ring had a larger distance from the metal center than the other metal-histidine complexes. There seems to be a desire of the copper molecule in both the single histidine complex and the dual histidine complex to work toward a square planar-type bonding than the octahedral type.

The free energy of reactions for the production of this dual histidine-metal complex from hydrated metal ions was calculated for all three metals. As with the previous free energy calculations, in order to approximate solvent effect on the free energy, the thermodynamic cycle was employed for this reaction (Fig. 8):

The results of the calculations are presented in Table 5. The nickel and the copper complexes again show reasonable favorability due to the spontaneous nature of the reaction. The free energy of reaction for the nickel and the copper dual histidine complexes is close to one another as was the case in the single histidine complex. The free energy of reaction for the dual histidine complexes when compared directly with the single histidine complexes shows that, in both cases, the free energy to form the dual histidine complex is lower than that of the single histidine complexes. The dual histidine zinc complexes were also negative like the complexes with nickel and copper. This is in contrast to the free energy with the single histidine, which was positive. The complexation of the zinc ion with two histidines is more thermodynamically favored than that of the single histidine complex.

Table 5 Free energy of reaction for the reaction: $M(H_2O)_6^{2+} + 2His^- \rightarrow M(His)_2 + 6H_2O$, B3LYP/6-311G(d), with SMD

Metal	ΔG(gas)	ΔG(solv)	ΔG(aq)
Ni^{2+}	−325.69	280.40	−45.29
Cu^{2+}	−336.14	296.20	−39.94
Zn^{2+}	−318.56	289.21	−29.35

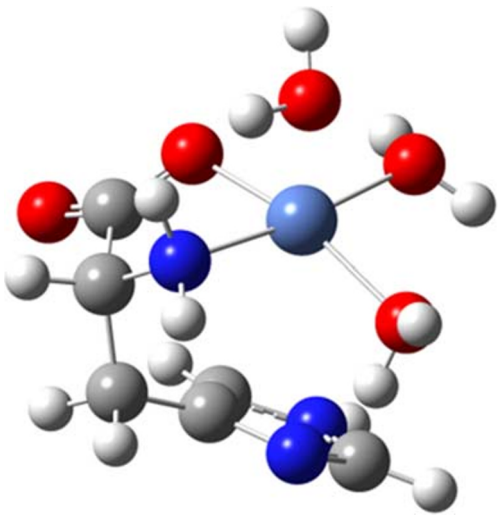

Fig. 9 The optimized structure of the adiabatic reduced single histidine-Ni complex and water molecules

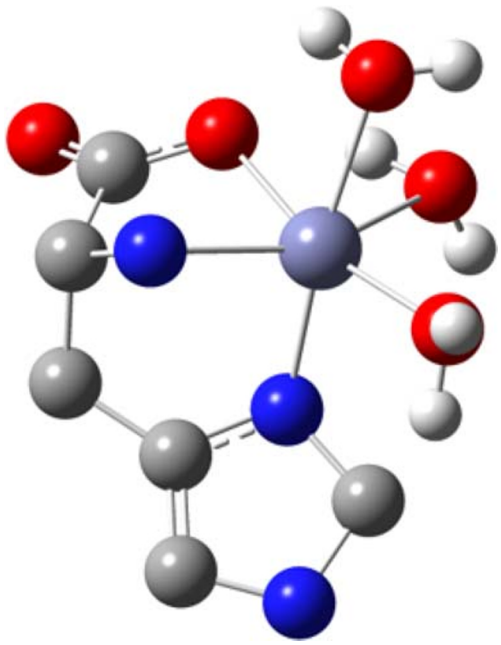

Fig. 10 The optimized structure of the adiabatic reduced single histidine-Zn complex and water molecules (hydrogen was removed from histidine for clarity)

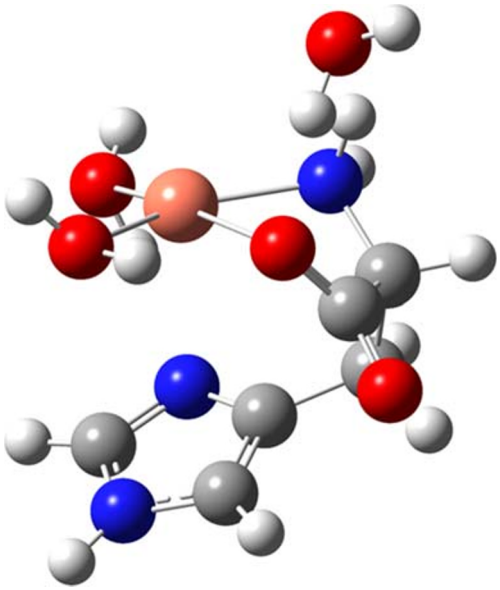

Fig. 11 The optimized structure of the adiabatic reduced single histidine-Cu complex and water molecules

One-electron reduction potentials and potential reaction pathways

Because of the various spin states and the ability of these ions to undergo reduction and oxidation that can cause biological damage, reduction potential of the single histidine-metal complex was calculated and presented in this work. Each of the metal ion complexes, when fully optimized with the additional electron, yielded significantly different geometric structures. The Adiabatic reduced structure of the nickel complex shifted from an octahedral complex to a square planar geometry (Fig. 9). The zinc complex did not change as significantly, but did experience an elongation of some bonds (Fig. 10). Cu makes the most significant changes with the addition of the extra electron (Fig. 11). Primarily, the imidazole completely disengages from the metal, along with one of the water molecules, to adopt the square planar conformation, instead of the octahedral.

Given that the reduction potential is the measure of the tendency of the ion to gain an electron, the more positive the reduction potential, the more likely it is that the ion gains the electron and be reduced. The reduction potential is calculated using the Nernst equation:

$$E = -\Delta G_{(aq)}/nF$$

where E is the reduction potential, n is the number of electrons being transferred ($n = 1$ in this case), and F is Faraday's constant of 96,500. The $\Delta G_{(aq)}$ is determined using the above equation with the thermodynamic cycle (Fig. 12):

The results are presented in Table 6. All of the metal ion complexes with one histidine show a tendency to attract electrons and be reduced. These complexes all have positive reduction potentials. A trend emerges as the metals increase in atomic number. As the atomic number increases among these three ions, the more likely the complex will be reduced. The zinc ion shows a relatively large reduction potential. This suggests that all of these complexes can participate in reactions that require it to attract electrons within biological systems but is unlikely to donate electrons to other reactants. Therefore, these complexes may cause biological damage by attracting electrons from other biological compounds or structures but will not initiate free radical formation via the donations of electrons from their complexes.

Table 6 1-electron reduction potential (in V) of $M(His)(H_2O)_3^+$

Metal	Reduction potential (in V)
$Ni(His)(H_2O)_3^+$	1.10
$Cu(His)(H_2O)_3^+$	3.00
$Zn(His)(H_2O)_3^+$	4.64

Conclusions

The authors of this work present a DFT study of 6-coordinated metal ion complexes with single histidine and dual histidines. This work presents both the geometric and energetic results of these calculations. The conclusions are as follows:

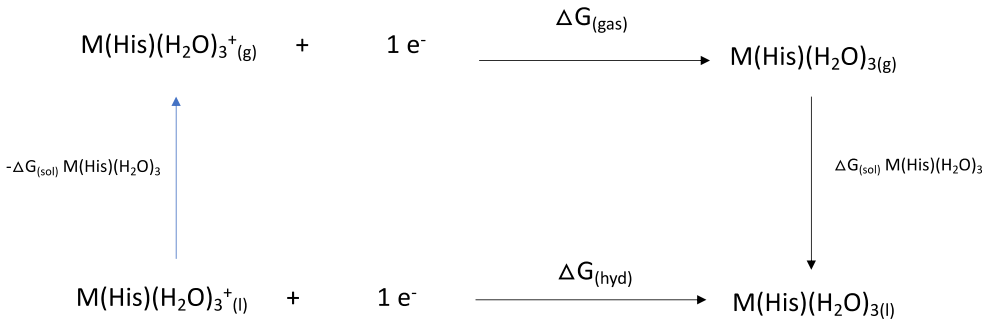

Fig. 12 The thermodynamic cycle for the 1-electron reduction of $M(His)(H_2O)_3^+$

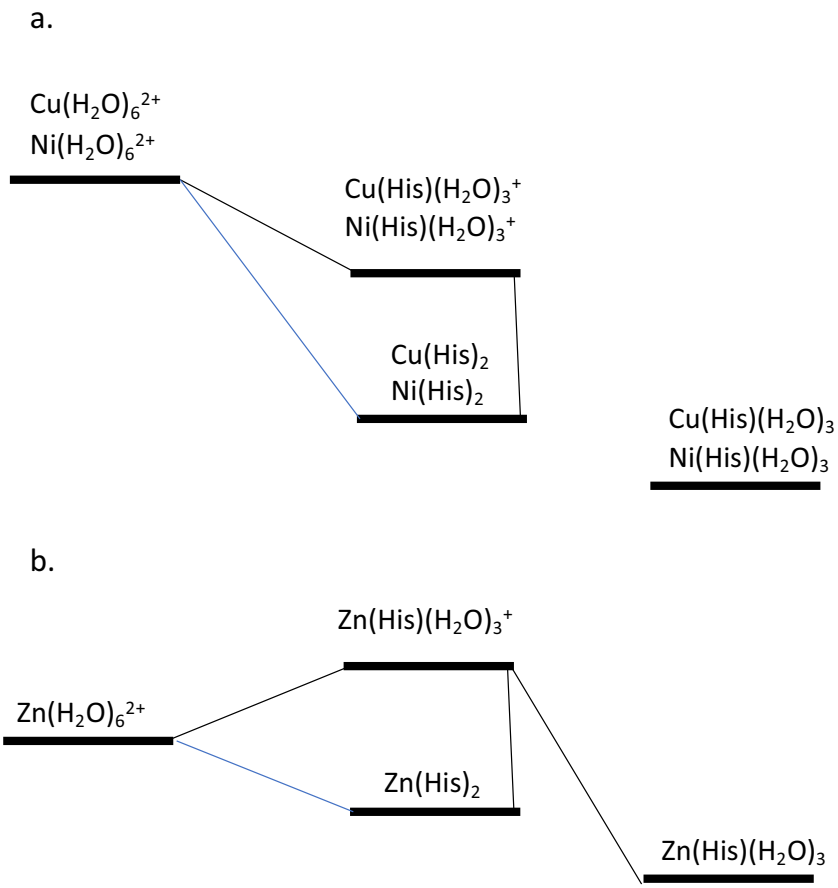

Fig. 13 An energy schematic showing the relative free energy of reaction for the complexes $M(H_2O)_6^{2+}$, the mono-histidine complex $M(His)(H_2O)_3^{+}$, the dual-histidine complexes, $M(His)_2$, and the reduced complexes. (M = Ni, Cu, Zn)

1. Figure 13 gives an overall concept of how these complexes may interact with each other. In nickel and copper complexes (Fig. 13a), the hydrated ion is thermodynamically favored to undergo both reactions, although the dual histidine complex is lower in energy than the single histidine-metal complex. If the reaction does drive toward the single histidine-metal complex, then, the reduced form is also thermodynamically favored to occur. The reduced form of the single histidine-metal complex is lower in energy than both the regular form of the single histidine-metal complex and the dual histidine-metal complex. This suggests that the reduced form of these complexes must be oxidized first before they can complex to the second histidine.
2. Figure 13b also shows that the zinc metal ion is thermodynamically unfavored to have a single histidine reaction. The hydrated zinc is, however, thermodynamically favored to undergo the reaction with the two histidines complex. The reduced form of the single histidine complex with zinc is lower in energy than all of the other zinc complexes. This suggests that if the zinc complex does react to produce the single histidine-metal complex, it is significantly thermodynamically favored to add an electron and go to the reduced state.
3. Copper exhibits Jahn-Teller distortions of the geometry in both the single and dual histidine-metal complexes, causing greater distance and less interaction of the metal ion with the imidazole side chain of the histidine in both. This is also shown by the movement of one water molecule away from the ion into a second level hydration shell.
4. The 1-electron reduction potential for all of the single histidine-metal complexes shows considerable likelihood to undergo redox reactions that add electrons to the complexes, reducing the metals. The addition of the electron causes small geometric changes within the zinc histidine complex. It causes significant change in the nickel and copper histidine complexes. The latter two move toward square planar conformation, releasing a water molecule and its attraction to the imidazole of the histidine.
5. B3LYP/6-311G(d) provide reasonable and cost-effective methods to study these complexes. The results compare favorably with available experimental and theoretical results. The use of SMD also proves to be adequate in the prediction of changes within an aqueous environment.
6. Finally, the free energies of reaction for all of the species are presented. Each of the reaction is favorable, thermodynamically, except for the formation of the single histidine zinc complex. This reaction is nonspontaneous, and therefore not favored to occur. If it does occur, the free

energy suggests it is highly favored to be reduced. The presence of the reduced form of the single histidine complex, although maintaining a high reduction potential, is unlikely to be observed due to the nonspontaneous nature of single histidine zinc complex formation.

Funding information The authors wish to recognize the support of the National Science Foundation HRD 1547754 and DMR 1826886.

References

1. Farkas E, Sovago I Metal complexes of amino acids and peptides. In: Ryadnov M, Hudecz F (eds) Amino acids, peptides and proteins, vol 412017, pp 100–151
2. Belal AAM, El-Deen IM, Farid NY, Zakaria R, Refat MS (2015) Synthesis, spectroscopic, coordination and biological activities of some transition metal complexes containing ONO tridentate Schiff base ligand. Spectrochim Acta A 149:771–787
3. Bieske EJ, Dopfer O (2000) High-resolution spectroscopy of cluster ions. Chem Rev 100:3963–3998
4. Care A, Bergquist PL, Sunna A (2015) Solid-binding peptides: smart tools for nanobiotechnology. Trends Biotechnol 33:259–268
5. Hashimoto Y, Yoshinari N, Matsushita N, Konno T (2014) Close correlation between metal oxidation states and molecular structures in a cobalt-gold multinuclear coordination system with mixed D-penicillaminate and tripodal triphosphine. Eur J Inorg Chem:3474–3478
6. Abdel-Rahman LH, El-Khatib RM, Nassr LAE, Abu-Dief AM, Ismael M, Seleem AA (2014) Metal based pharmacologically active agents: synthesis, structural characterization, molecular modeling, CT-DNA binding studies and in vitro antimicrobial screening of iron (II) bromosalicylidene amino acid chelates. Spectrochim Acta A 117:366–378
7. Gutierrez A, Gracia-Fleta L, Marzo I, Cativiela C, Laguna A, Gimeno MC (2014) Gold(I) thiolates containing amino acid moieties. Cytotoxicity and structure-activity relationship studies. Dalton Trans 43:17054–17066
8. Moustafa EM, Korany M, Mohamed NA, Shoeib T (2014) Carnosine complexes and binding energies to some biologically relevant metals and platinum containing anticancer drugs. Inorg Chim Acta 421:123–135
9. Guo CX, Li P, Pei MS, Zhang GY (2015) A new polythiophene derivative-based fluorescent sensor for Co2+, Cu2+, Cd2+, and its complex with Cu2+ for sensing homocysteine and glutathione. Sensors Actuators B Chem 221:1223–1228
10. Arun TR, Raman N (2014) Antimicrobial efficacy of phenanthrenequinone based Schiff base complexes incorporating methionine amino acid: structural elucidation and in vitro bio assay. Spectrochim Acta A 127:292–302
11. Ding XZ, Hua YF, Chen YM, Zhang CM, Kong XZ (2015) Heavy metal complexation of thiol-containing peptides from soy glycinin hydrolysates. Int J Mol Sci 16:8040–8058
12. Ghosh C, Seal M, Mukherjee S, Dey SG (2015) Alzheimer's disease: a heme-A beta perspective. Acc Chem Res 48:2556–2564
13. Grasso G, Bonnet S (2014) Metal complexes and metalloproteases: targeting conformational diseases. Metallomics 6:1346–1357
14. Hussien MA, Nawar N, Radwan FM, Hosny NM (2015) Spectral characterization, optical band gap calculations and DNA binding of some binuclear Schiff-base metal complexes derived from 2-aminoethanoic acid and acetylacetone. J Mol Struct 1080:162–168
15. Ali-Torres J, Mirats A, Marechal JD, Rodriguez-Santiago L, Sodupe M (2014) 3D structures and redox potentials of Cu2+-A beta(1-16) complexes at different pH: a computational study. J Phys Chem B 118:4840–4850
16. Breivogel A, Kreitner C, Heinze K (2014) Redox and photochemistry of bis (terpyridine) ruthenium (II) amino acids and their amide conjugates-from understanding to applications. Eur J Inorg Chem: 5468–5490
17. Gao YP, Wang YY, Liu WX (2015) Redox activity of the mini-alpha A-crystallin-Cu (II) complex and its biological relevance. Int J Electrochem Sci 10:6302–6311
18. Kepp KP (2012) Bioinorganic chemistry of Alzheimer's disease. Chem Rev 112:5193–5239
19. Chen WT, Liao YH, Yu HM, Cheng IH, Chen YR (2011) Distinct effects of Zn2+, Cu2+, Fe3+, and Al3+ on amyloid-beta stability, oligomerization, and aggregation. J Biol Chem 286:9646–9656
20. Bush AI, Pettingell WH, Multhaup G, Paradis MD, Vonsattel JP, Gusella JF, Beyreuther K, Masters CL, Tanzi RE (1994) Rapid induction of Alzheimer A-beta amyloid formation by zinc. Science 265:1464–1467
21. Goedert M, Spillantini MG (2006) A century of Alzheimer's disease. Science 314:777–781
22. Hardy J, Selkoe DJ (2002) Medicine-the amyloid hypothesis of Alzheimer's disease: progress and problems on the road to therapeutics. Science 297:353–356
23. Grenacs A, Sanna D, Sovago I (2015) Copper (II) and nickel (II) binding sites of peptide containing adjacent histidyl residues. J Inorg Biochem 151:87–93
24. Guilloreau L, Damian L, Coppel Y, Mazarguil H, Winterhalter M, Faller P (2006) Structural and thermodynamical properties of Cu-II amyloid-beta 16/28 complexes associated with Alzheimer's disease. J Biol Inorg Chem 11:1024–1038
25. Mantyh PW, Ghilardi JR, Rogers S, Demaster E, Allen CJ, Stimson ER, Maggio JE (1993) Aluminum, iron, and zinc ions promote aggregation of physiological concentrations of beta-amyloid peptide. J Neurochem 61:1171–1174
26. Nunomura A, Perry G, Aliev G, Hirai K, Takeda A, Balraj EK, Jones PK, Ghanbari H, Wataya T, Shimohama S, Chiba S, Atwood CS, Petersen RB, Smith MA (2001) Oxidative damage is the earliest event in Alzheimer disease. J Neuropathol Exp Neurol 60:759–767
27. Huang XD, Atwood CS, Hartshorn MA, Multhaup G, Goldstein LE, Scarpa RC, Cuajungco MP, Gray DN, Lim J, Moir RD, Tanzi RE, Bush AI (1999) The A beta peptide of Alzheimer's disease directly produces hydrogen peroxide through metal ion reduction. Biochemistry 38:7609–7616
28. Masters CL, Simms G, Weinman NA, Multhaup G, McDonald BL, Beyreuther K (1985) Amyloid plaque core protein in Alzheimer disease and down syndrome. Proc Natl Acad Sci U S A 82:4245–4249
29. Kong XT, Zhao Z, Lei X, Zhang BB, Dai DX, Jiang L (2015) Interaction of metal ions with the His13-His14 sequence relevant to Alzheimer's disease. J Phys Chem A 119:3528–3534
30. Pushie MJ, Nienaber KH, McDonald A, Millhauser GL, George GN (2014) Combined EXAFS and DFT structure calculations provide structural insights into the 1:1 multi-histidine complexes of Cu-II, Cu-I, and Zn-II with the tandem octarepeats of the mammalian prion protein. Chem Eur J 20:9770–9783
31. Han GC, Ferranco A, Feng XZ, Chen ZC, Kraatz HB (2014) Synthesis, characterization of some ferrocenoyl cysteine and histidine conjugates, and their interactions with some metal ions. Eur J Inorg Chem:5337–5347
32. Potocki S, Valensin D, Kozlowski H (2014) The specificity of interaction of Zn2+, Ni2+ and Cu2+ ions with the histidine-rich domain of the TjZNT1 ZIP family transporter. Dalton Trans 43: 10215–10223

33. Umadevi P, Senthilkumar L (2014) Influence of metal ions (Zn2+, Cu2+, Ca2+, Mg2+ and Na+) on the water coordinated neutral and zwitterionic L-histidine dimer. RSC Adv 4:49040–49052
34. Gorboletova GG, Metlin AA (2014) Thermodynamics of the formation of nickel (II) complexes with L-histidine in aqueous solutions. Russ J Phys Chem A 88:1514–1518
35. Chen LT, Liu T, Ma C (2010) Metal complexation and biodegradation of EDTA and S,S-EDDS: a density functional theory study. J Phys Chem A 114:443–454
36. Sillanpaa AJ, Aksela R, Laasonen K (2003) Density functional complexation study of metal ions with (amino) polycarboxylic acid ligands. Phys Chem Chem Phys 5:3382–3393
37. Frisch MJ, Trucks GW, Schlegel HB, Scuseria GE, Robb MA, Cheeseman JR, Scalmani G, Barone V, Petersson GA, Nakatsuji H, Li X, Caricato M, Marenich AV, Bloino J, Janesko BG, Gomperts R, Mennucci B, Hratchian HP, Ortiz JV, Izmaylov AF, Sonnenberg JL, Williams FD, Lipparini F, Egidi F, Goings J, Peng B, Petrone A, Henderson T, Ranasinghe D, Zakrzewski VG, Gao J, Rega N, Zheng G, Liang W, Hada M, Ehara M, Toyota K, Fukuda R, Hasegawa J, Ishida M, Nakajima T, Honda Y, Kitao O, Nakai H, Vreven T, Throssell K, Montgomery Jr JA, Peralta JE, Ogliaro F, Bearpark MJ, Heyd JJ, Brothers EN, Kudin KN, Staroverov VN, Keith TA, Kobayashi R, Normand J, Raghavachari K, Rendell AP, Burant JC, Iyengar SS, Tomasi J, Cossi M, Millam JM, Klene M, Adamo C, Cammi R, Ochterski JW, Martin RL, Morokuma K, Farkas O, Foresman JB, Fox DJ (2016) Gaussian 16 Rev. C.01, Wallingford, CT
38. Becke AD (1993) Density-functional thermochemistry. 3. The role of exact exchange. J Chem Phys 98:5648–5652
39. Lee CT, Yang WT, Parr RG (1988) Development of the Colle-Salvetti correlation-energy formula into a functional of the electron density. Phys Rev B 37:785–789
40. Roy Dennington TAK, Millam JM (2016) GaussView, version 6.1. Semichem Inc., Shawnee Mission, KS
41. Marenich AV, Cramer CJ, Truhlar DG (2009) Universal solvation model based on solute electron density and on a continuum model of the solvent defined by the bulk dielectric constant and atomic surface tensions. J Phys Chem B 113:6378–6396